

Time Lag between Accretion and Wind Events in the T Tauri Star RY Tau

E. V. Babina,^{1,*} P. P. Petrov,¹ K. N. Grankin,¹ S. A. Artymenko¹

¹*Crimean Astrophysical Observatory, Republic of Crimea, 298409, Russia*

The results of spectroscopic and photometric monitoring of the classical T Tauri star RY Tau are presented. The observation series span 220 nights from 2013 to 2024. During the observation period, the star's brightness varied within the range of $V=9\text{--}11^m$. The rotation axis of the "star + accretion disk" system is tilted at a large angle, so the line of sight intersects the wind region and accreting flows in the star's magnetosphere. Variability in the short-wavelength wing of the $\text{H}\alpha$ emission line and the profile of the D NaI resonance doublet are analyzed. It is shown that the wind and accretion flows vary on a time scale of approximately 20 days. When the predominant flow direction changes, a time lag is observed: initially, accretion increases, and after two days, absorption in the line-of-sight wind decreases. It is concluded that the spectral line profiles are formed in the magnetospheric accretion flows and the *conical wind* originating from the boundary of the star's magnetosphere. The time lag is determined by the tilt of the magnetic dipole and the opening angle of the conical wind. It is assumed that RY Tau operates in an unstable propeller mode, and fluctuations in the accretion and wind flows are caused by density waves in the accretion disk.

Keywords: Stars: variables: T Tauri, Herbig Ae/Be – Stars: winds, outflows – Line: profiles – Stars: individuals: RY Tau

1. INTRODUCTION

Classical T Tauri variables (CTTS) are young, low-mass stars ($\leq 2M_\odot$) with accretion disks that show both signs of ongoing accretion and signs of an intense wind. The magnetospheric accretion model (Camenzind 1990, Hartmann et al. 1994, Koenigl 1991, Shu et al. 1994) most successfully explains the spectral features of these stars, including the emission line profiles indicating line-of-sight gas flows toward the star (accretion) and away from the star (wind) (Alencar and Basri 2000). According to this model, disk accretion onto the young star is stopped by the star's magnetic field at a distance determined by the accretion rate and the strength of the dipole component of the stellar magnetic field. From this distance, free fall of gas occurs onto the star's surface along the magnetospheric field lines. At the impact site, a shock wave with a temperature of $\sim 10^6$ K is generated on the star's surface. A significant portion of the shock wave's UV radiation is concentrated in the $\text{Ly}\alpha$ emission line (Arulanantham et al. 2023). The X-ray and UV radiation from the shock wave ionizes gas in the star's vicinity and heats the underlying region of the photosphere

the hot spot. The hot spot radiation explains the observed UV excess in the energy distribution in the CTTS spectrum and the veiling effect of photospheric lines (Dodon and Lamzin 2012). The CTTS accretion rate is $10^{-8}\text{--}10^{-9} M_\odot/\text{yr}$ (Bouvier et al. 2007).

In addition, CTTSs exhibit a strong wind. The mass loss rate is, on average, an order of magnitude smaller than the accretion rate. Various wind models have been considered: a disk wind accelerated by the magnetic centrifuge of a rotating disk (Romanova and Owocki 2015, Shu et al. 1994, Ustyugova et al. 2006), a conical wind starting at the accretion disk-magnetosphere boundary and accelerated by magnetic pressure (Romanova et al. 2009), a polar wind accelerated by MHD waves that arise during gas accretion onto the stellar surface (Crammer 2008), and others.

Analysis of CTTS emission spectra shows that both the accretion flows and the wind region are heterogeneous: the accretion flows contain streams of increased density, while the wind contains clouds of higher density compared to the surrounding flows (Fischer et al. 2008, Kwan and Fischer 2011). At large distances, the wind is collimated by the magnetic field into bipolar jets (see review by Pascucci et al. (2023)).

Reviews of the observed characteristics of

* helenka_truth@mail.ru

CTTS can be found in Hartmann et al. (2016), Bouvier et al. (2007), Petrov (2021).

Spectral observations of CTTSs allow us to “visualize” gas flows and measure infall and outflow velocities using Doppler-broadened spectral line profiles, and track how the dynamics of these processes change over different time scales—from days to years. For this purpose, monitoring of selected objects is being conducted. The most dense series of observations of CTTS AA Tau were conducted simultaneously at several observatories (Bouvier et al. 2003). Spectroscopic and photometric observations of CTTSs spanning several years were conducted for the stars SU Aur – Giampapa et al. (1993), Johns and Basri (1995), Petrov et al. (2019, 1996); RY Tau – Babina et al. (2016), Petrov et al. (2019); RW Aur – Alencar et al. (2005), Petrov et al. (1996), Takami et al. (2016); DR Tau – Alencar et al. (2001).

In this paper, we present the results of our 11-year series of observations of RY Tau, from 2013 to 2024. The goal of this study is to determine the timing characteristics and identify causal relationships in accretion and wind events. RY Tau is one of the brightest and most frequently observed CTTSs in the northern sky. The main parameters of the star, according to Calvet et al. (2004), are $T_e=5945\pm142$ K, $L_*=9.6\pm1.5$ L_\odot , $M_*=2.0\pm0.3$ M_\odot , $R_*=2.9\pm0.4$ R_\odot .

The star is visible at a large inclination of its rotation axis to the line of sight; however, no periodic variability caused by the star’s axial rotation can be observed (Zajtseva 2010). The magnetic dipole is likely not tilted to the star’s rotation axis. The projected rotation velocity $v \sin i$, determined from photospheric lines, is 52 ± 2 km s^{-1} (Bouvier 1990, Petrov et al. 1999). Knowing the star’s radius, the projected rotation velocity $v \sin i$, and the tilt angle i , we can estimate the rotation period: $P_*=2.84\pm0.40$ d , i.e., RY Tau belongs to the rapidly rotating CTTS. The corresponding corotation radius in the protoplanetary disk of RY Tau is $10\pm1R_\odot$.

The protoplanetary disk of RY Tau is well resolved by the ALMA interferometer; the disk rotation axis is tilted at 65° to the line of sight (Long et al. 2019). The tilt of the inner disk,

determined from K-band interferometry, $i=60^\circ$ (Perraut et al. 2021). At a tilt angle of $60\text{--}65^\circ$, the line of sight intersects the disk wind and the star’s magnetosphere. The observed photometric variability of RY Tau is likely largely due to absorption in the dusty disk wind (Babina et al. 2016, Davies et al. 2020).

Irregular brightness increases occurred in 1983–1984 and 1996–1997 (Herbst et al. 1994, Herbst and Stine 1984, Zajtseva et al. 1996). The longest series of photometric observations of RY Tau, from 1965 to 2000, was analyzed by Zajtseva (2010): quasi-periodic brightness variations were detected, presumably caused by eclipses by a dust cloud in the circumstellar disk. No periodicity associated with the axial rotation of the star was detected.

Photometric observations of RY Tau from 1983–2004 revealed a period of 377 ± 10 days. It has been suggested that this period is caused by the presence of forming bodies in the protoplanetary disk (Ismailov and Adygezalzade 2012). A period of 23 days was detected in variations of the MgII 2800 Å emission line in the ultraviolet spectrum of RY Tau (Ismailov et al. 2015). Similar period values were also found in a series of photometric observations (Bouvier et al. 1993, Gahm et al. 1993).

In addition, observations from 2013 to 2020 revealed variations in the H α flux at a radial velocity of $RV=-95\pm5$ km s^{-1} with a period of 21.6 days. These were interpreted as density streams in the disk wind caused by the inhomogeneous structure of the protoplanetary disk at a distance of ~0.2 AU from the star (Petrov et al. 2023, 2021).

RY Tau exhibits an extended jet containing knots with a dynamical age of less than 10 years (Agra-Amboage et al. 2009, Skinner et al. 2018, St-Onge and Bastien 2008, Takami et al. 2023). The jet is warped, which may be due to the tilt of the accretion disk caused by the presence of a planet or a low-mass component of the star (Garufi et al. 2019). RY Tau is a source of variable X-ray emission, indicating the presence of hot plasma with a temperature of $T\approx50$ MK (Skinner et al. 2016).

2. OBSERVATIONS

The bulk of our spectral observations of RY Tau were carried out at the Crimean Astrophysical Observatory (CrAO RAS) using the 2.6-m ZTSh telescope and the ESPL spectrograph (Lagutin et al. 2020). The spectral resolution was $\lambda/\Delta\lambda \approx 27000$ with an entrance slit width of 2 arcseconds. Spectral regions in the H α and D NaI lines were analyzed. Spectral observations were also conducted at the Kourovka Observatory of UrFU using the 1.21-m telescope ($\lambda/\Delta\lambda \approx 27000$) and, during one season (2015-2016), using the 2.5-m NOT telescope, $\lambda/\Delta\lambda \approx 15000$, and the 2.2-m CAHA telescope, $\lambda/\Delta\lambda \approx 30000$ (Spain).

Since we measure fairly broad spectral line profile details (see the next section), the difference in spectral resolution between the different instruments was insignificant.

Photometric observations of RY Tau in the BVRI system were conducted on the same nights as the spectroscopic observations using telescopes of the Crimean Astrophysical Observatory, primarily the 1.25-m AZT-11 telescope. Several brightness estimates were obtained using the 0.8-m RK-800 telescope. The typical accuracy of photometric measurements of the star's brightness was $\pm 0.02^m$ in each band. In cases when weather conditions prevented precise photometry, we used the AAVSO database (<https://www.aavso.org>). In general, good agreement (within $\pm 0.02^m$) between our brightness estimates and the photometric data from the AAVSO database should be noted.

A more detailed description of the observations and analysis of the results were presented in our previous publications (Babina et al. (2016), Petrov et al. (2023, 2019, 2021)). In total, our observations of RY Tau cover 220 nights over 11 seasons from 2013 to 2024.

3. OBSERVATION ANALYSIS

We used the H α emission line and the D absorption lines of the NaI doublet to analyze the accretion and wind dynamics along the line of sight. The limited size of the imaging detector

in the ESPL spectrograph prevented us from simultaneously recording other accretion and wind indicators, such as HeI 5876 Å or the infrared CaII triplet lines. Figure 1 shows the most characteristic H α and D line profiles, arranged (from top to bottom) in order of decreasing wind signatures and increasing accretion signatures. All spectra shown in this article are displayed on an astrocentric wavelength and radial velocity scale. The radial velocity of RY Tau is assumed to be $+18 \text{ km s}^{-1}$. Observation dates are given in the HJD-2450000 format. The radial velocity scale in the NaI doublet line region is given relative to the D1 line.

H α emission is formed both in the stellar magnetosphere and in wind streams (Kwan and Fischer 2011, Muzerolle et al. 2001). The profiles of the hydrogen Balmer lines in different CTTS wind models were studied in Kurosawa et al. (2011). The characteristic depression of the H α profile in the shortwave wing of the line is an indicator of absorption in the line-of-sight wind. In the spectra of RY Tau, this depression sometimes shifts toward the line center and even into the longwave wing, indicating absorption in the gas flow infalling onto the star during periods of enhanced accretion (see Fig. 1, HJD 8410 and 8414).

Absorption lines of the D NaI resonance doublet are formed both in infalling gas streams within the magnetosphere and in the densest regions of the wind (Calvet et al. 2004). Absorption in the “blue” wing of the D NaI lines, which characterizes absorption in the wind, extends to velocities exceeding 200 km s^{-1} . In the D1 line, the “red” wing is partially blended with telluric water lines, and in the more saturated D2 line, on observation dates when wind signatures were minimal, the “red” wing extended to velocities of $\sim 250 \text{ km s}^{-1}$ (see Fig. 1), which characterizes the gas infall velocity. The maximum infall velocity can be used to estimate the magnetospheric radius R_m (see, e.g., Takasao et al. 2022). Taking into account the uncertainties in the mass and radius of RY Tau, $R_m=10\pm4 R_\odot$.

It should be noted that under magnetospheric conditions, sodium atoms are almost completely ionized, so the absorption profile in the D NaI lines reflects the dynamics of the densest regions,

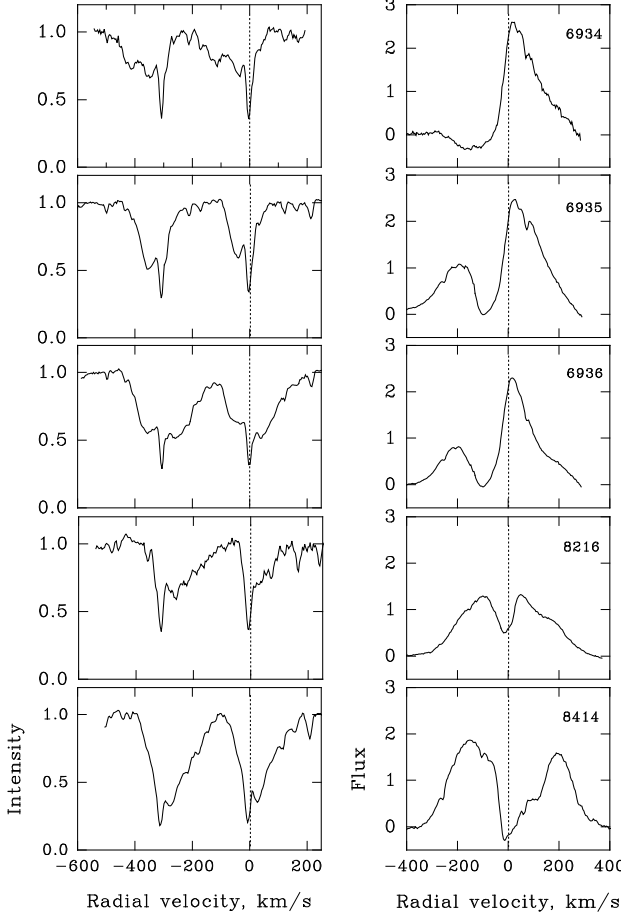


Figure 1. Examples of NaI D (left panel) and H α (right panel) line profiles. Observation dates (HJD-2450000) are indicated in the upper right corner of the right panel. The H α line flux is given in units of $3.67 \cdot 10^{-13}$ erg cm $^{-2}$ s $^{-1}$.

where the fraction of neutral atoms is still quite high. The velocity measured from the extent of the “red” wing of these lines can be considered the lower limit of the velocity of gas infall onto the star’s surface.

The D NaI line profiles also contain a narrow interstellar absorption band at a radial velocity of about -10 km s $^{-1}$ relative to the star.

When analyzing the variability of the H α and D NaI line profiles, we chose the following parameters: (see Fig. 2) F_b and F_r are the radiative fluxes in the “blue” and “red” halves of the profile, relative to zero radial velocity. The radiative flux was calculated from the equivalent line width EW and the stellar magnitude V at the time of observation: $F = EW(\text{\AA}) \cdot 10^{-0.4(V-10)}$, in

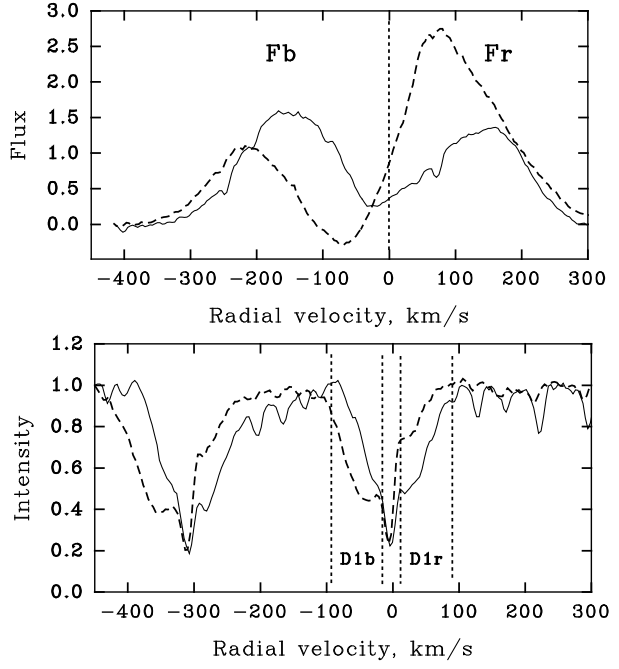


Figure 2. Profiles of the H α and D NaI lines. Observation times: HJD 8734 (solid line) and 8765 (dashed line).

units of $3.67 \cdot 10^{-13}$ erg cm $^{-2}$ s $^{-1}$.

The unit of measurement is the continuum flux of a 10th-magnitude star in the V band. It would be more appropriate to use the photometric magnitude R, but for some observation dates, only the magnitude V was available in the AAVSO database. Using the magnitude V to determine the H α flux yields a systematic error of no more than 10%, since as the brightness of RY Tau varies within the range of $V=9.6$ - 11.0^m , the color (V-R) remains almost constant: 1.1 ± 0.1^m (Petrov et al. 2019).

Changes in the F_b flux reflect changes in the wind density along the line of sight. The parameter F_r characterizes the emission of the magnetosphere and wind in the H α line. In the D1 NaI line profile, we measured the equivalent width of the “blue” and “red” absorption wings of the D1 line, each 1.5\AA (76 km s $^{-1}$) long, excluding the central region where the narrow interstellar absorption is located (see Fig. 2).

The D1r parameter characterizes the absorption in the magnetospheric flux incident on the star, while the D1b parameter characterizes the absorption in the wind outside the magneto-

sphere, likely at the wind base or in the densest wind streams or clouds.

Figure 3 shows how the star's V brightness, total H α flux, and D1r absorption, which characterizes accretion, changed over time. During minimal accretion (HJD 7650 – 7657), the minimum H α flux and minimum V brightness were observed. Observations were performed over seven consecutive nights, and throughout the entire period, the spectral line profiles showed signs of a strong wind with velocity up to 200 km s $^{-1}$ and no signs of accretion (EW D1r \approx 0).

During other continuous observation intervals, noticeable changes in the accretion and wind fluxes occurred on time scales of a day or longer (see, for example, Fig. 1).

It should be noted that the variations in the aforementioned spectral line parameters (Fb, Fr, D1b, D1r) do not reveal the star's rotation period. During some continuous observation intervals lasting 6 days (approximately two stellar rotations), there were no significant changes in the line profiles. This indicates that the gas fluxes – accreting or outflowing – are *axially symmetric*. On the observation dates of HJD 8215 and 8216 (Fig. 1), the strongest signs of accretion are visible in the D NaI line profile. The H α profile on these dates showed absorption at the line center. At another day, HJD 8410, the absorption is clearly shifted to the “red” wing of the H α line, indicating gas infall onto the star.

Of the four parameters – Fb, Fr, D1b and D1r – a correlation is observed only between two parameters, D1r (accretion) and Fb (wind): as accretion (D1r) increases, the wind speed decreases, and the depression in the blue H α wing shifts toward the line center (see Fig. 1), resulting in an increase in the Fb flux – accretion dampens the wind (Fig. 4).

4. TIME SERIES CROSS-CORRELATION

We analyze the variability of observed parameters: the accretion signature (D1r) and the wind signature (Fb). These signatures are present in each spectrum, vary on a time scale of several days, and are significantly correlated. However, we do not know *a priori* whether the accretion

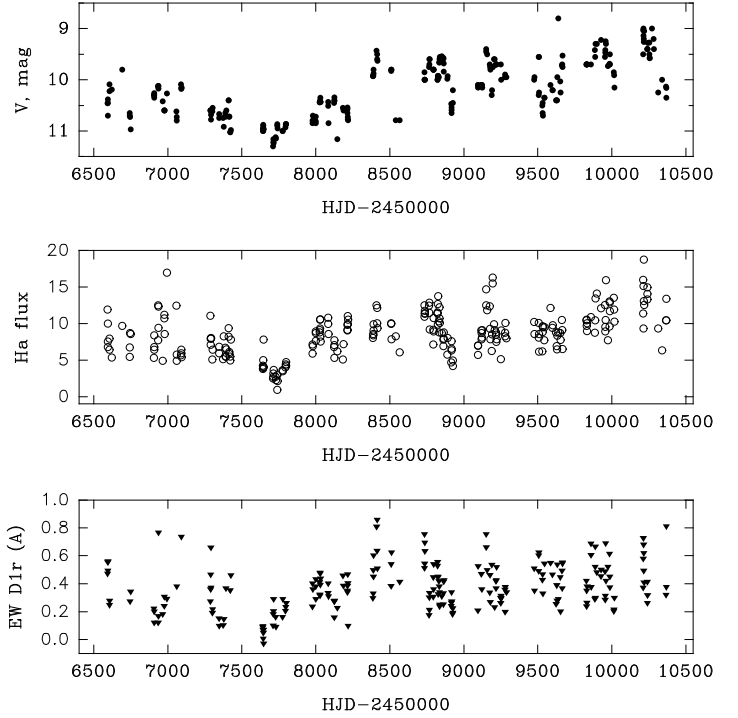


Figure 3. Variations in the star's V-band brightness, H α flux, and accretion flow absorption (EW D1r) over 11 years.

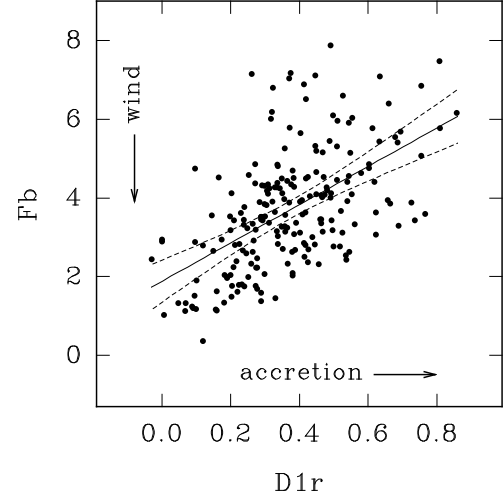


Figure 4. Correlation between the absorption in the accreting flow (D1r) and the emission flux (Fb) in the “blue” wing of the H α emission line. The dashed lines indicate the 99% confidence interval. Low Fb flux values correspond to high wind density along the line of sight. As accretion increases, the wind density decreases and the Fb flux increases.

and wind signatures change simultaneously, or whether changes in one spectral line occur a day or two earlier than in the other. For example, the accretion signature in the D NaI lines appears first, followed by changes in the wind signature in the H α line. We will test this hypothesis: first accretion, then wind.

We denote the variables: D1r is the redshifted absorption in the D1 NaI resonance line. The equivalent width of this absorption is measured in Angstroms. Another quantity is the radiation flux Fb in the short-wavelength wing of the H α emission profile.

Next, we use the time series cross-correlation method. We create a uniform data series [HJD, D1r] with a step of one day, and the same data series [HJD, Fb]. Dates on which there were no observations contain empty cells in the series. We plot a graph of Fb as a function of D1r and determine the correlation coefficient. Then, we shift the series [HJD, D1r] by one day relative to the series [HJD, Fb], so that the Fb parameter is compared with the D1r parameter on the previous day, plot the graph again, and determine the correlation coefficient. In this way, we check: will the correlation change if changes in the D NaI lines occur one day earlier than changes in H α . By shifting the data series in the other direction, we test the inverse hypothesis. This way, we determine what is the cause and what is the effect.

Since the characteristic timescale for changes in accretion and wind fluxes is several days, a positive correlation is observed at any shift: the stronger the accretion flux, the stronger the wind flux. However, the dispersion of data points on this curve is quite large. Using time series cross-correlation, we attempt to determine at what shift the maximum correlation is observed.

Our observations were conducted in short sets of 5-7 consecutive nights during each month, from September to March. Correlation in such fragmented data series can only be investigated with time series shifts of no more than ± 4 days. At zero shift, all observation nights are included in the correlation, but with a shift of 3-4 days, the number of data points is significantly reduced, increasing the error in determining the correlation coefficient.

Fig.5 shows how the correlation coefficient

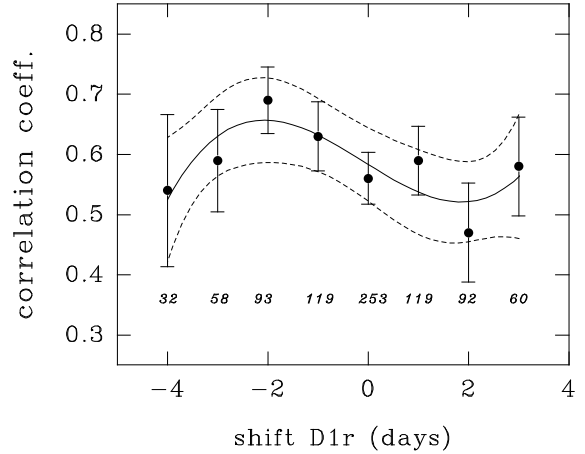


Figure 5. Cross-correlation of the [HJD, D1r] and [HJD, Fb] time series with a shift of one series relative to the other within the range of -4 to +3 days. The solid line is the approximation by a third-degree polynomial. The dotted lines show the 95% confidence interval. The maximum correlation corresponds to a shift of -2 days: first, the accretion changes, then the wind changes.

varies depending on the relative shift of the accretion and wind time series. The characteristic bend in this dependence (maximum at D1r = -2d and minimum at D1r = +2d) indicates that the accretion time series is shifted by two days relative to the wind time series, i.e. accretion events lead wind events. This suggests that accretion is the cause and wind is the effect.

The error bars shown in the figure are formally defined as $\sqrt{(1 - r^2)/(n - 2)}$, where r = correlation coefficient, n = number of measurements.

Fig.6 shows the relationship between accretion and wind parameters for different shifts of the [HJD, D1r] time series relative to the [HJD, Fb] time series. With a shift of 2 days, the number of data points involved in the correlation is significantly reduced, but the regression line remains within the confidence interval $>99\%$.

One might assume that this is an effect of the axial rotation of a star with an axially asymmetric magnetosphere: on one side, we observe dominant accretion, and after half a rotation of the star, we see dominant wind. However, in this case, we would register periodic variations in these spectral signatures with the rotation period of the star. However, no such periodicity

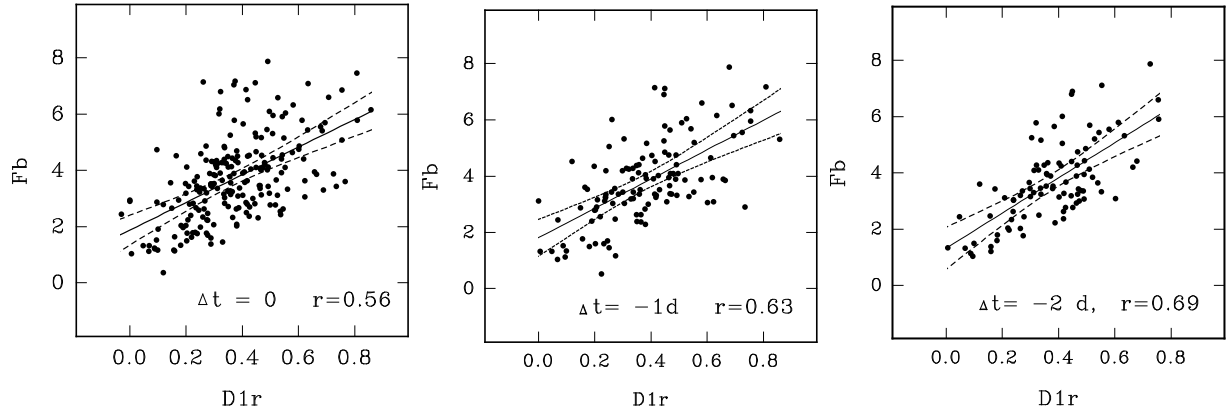


Figure 6. Correlation between the accretion (D1r) and wind (Fb) parameters at different time series shifts: the maximum correlation coefficient ($r = 0.69$) was obtained at $\Delta t = -2$ days: accretion changes first, and then the wind changes 2 days later. The dotted lines indicate the 99% confidence interval.

is observed. Frequency analysis shows that the variations in the accretion (D1r) and wind (Fb) parameters do not correspond to the rotation period of the star. And, as noted above, during continuous observation intervals of 6-7 days (two rotations of the star), there were no significant changes in the line profiles.

5. DISCUSSION

Correlations between CTTS accretion and wind events are detected in spectral monitoring programs. The most detailed study of this kind was conducted during observations of AA Tau (Bouvier et al. 2003). It was shown that the deformation of the star's magnetospheric field lines due to differential rotation of the magnetosphere and accretion disk leads to repeated magnetospheric reorganization and recovery events. This is reflected in the dynamics of the accretion and wind gas flows and manifests itself in variability in the emission line profiles in the star's spectrum (Bouvier et al. 2003). In the case of AA Tau, the characteristic timescale of such changes is approximately a month.

Unlike AA Tau, RY Tau is a more massive ($\sim 2M_{\odot}$) and rapidly rotating ($P \approx 3^d$) star. The magnetospheric radius is close to the corotation radius and possibly exceeds it. In this case, a magnetic propeller regime and a conical wind arise (Romanova et al. 2009). The conical wind originates from the magnetosphere

accretion disk boundary and is accelerated by the magnetic pressure gradient of the toroidal fields (Romanova et al. 2009, Takasao et al. 2022). As it moves away from the star, the conical wind collimates into a jet.

The observed correlation between the variations in accretion and wind fluxes in RY Tau indicates that the maximum wind density is located near the magnetospheric boundary. This supports the *conical* wind scenario. A disk wind originating from the more extended surface of the accretion disk could not provide the observed correlation between accretion and wind events on a two-day timescale. We are looking at the star through the conical wind envelope, seeing discrete events of gas accretion onto the star and the relatively rapid response of the wind to these events.

In the case of RY Tau, the observed delay in the wind's response to accretion changes can be explained by the wind's geometry. At the moment of accretion intensification, wind outflow at the magnetosphere's boundary ceases. Looking at the star at an angle of $60\text{--}65^{\circ}$ to the disk's rotation axis, we will see gas infall projected onto the star within a day, but the change in wind density along the line of sight will occur later, when the wind, originating from the magnetosphere's boundary, rises above the disk's surface and appears along the line of sight projected onto the star (see Fig. 7). At an average velocity of $\sim 100 \text{ km s}^{-1}$, the wind will travel a distance of

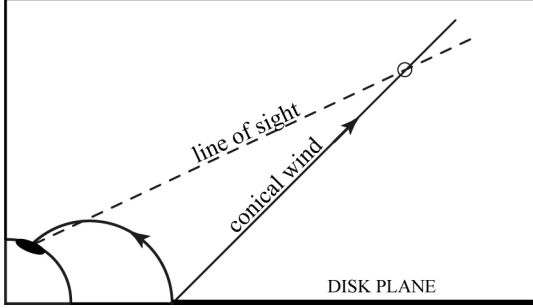


Figure 7. Star, magnetosphere, and the conical wind vector.

~ 0.11 AU in two days, which is approximately twice the radii of RY Tau’s magnetosphere.

Of particular interest is the fact that the dominant direction of gas flow along the line of sight (accretion or wind) varies with a characteristic time of approximately 20 days. During a single observation set (5-7 days), the flow direction generally remains constant, but during the time between sets (20-30 days), it almost always changes.

This is similar to the operation of an “unstable propeller”, where the radius of the magnetosphere is not constant. The radius of the magnetosphere is determined by the balance between the pressure of the star’s magnetic field ($\sim B^2/8\pi$) and the dynamic pressure of the gas flow ($\sim \rho v^2/2$) in the accretion disk. The star’s magnetic field (B) does not change as rapidly, but the gas density (ρ) at the inner boundary of the accretion disk can change because the disk is not uniform – the presence of forming planets in the disk causes density waves that reach the inner boundary of the disk (see, e.g., Armitage, 2010). Density changes affect the position of the magnetospheric boundary and, as a result, can alter the magnetic propeller regime.

The one-sided accretion scenario was also considered, where gas infalls onto the star from one side of the disk plane, while the wind (and jet) originates from the other side. These directions spontaneously switch with a characteristic time of approximately 30 days (result of 2D modeling, Lovelace et al. 2010). If the accretion disk contains a planet on an eccentric or inclined orbit, it can synchronize this process with the orbital period. In the case of RY Tau, a period of

21.6 days was observed in line-of-sight wind density variations based on observations from 2013 to 2020 (Petrov et al. 2021, see also Vedula and Johns-Krull 2024). A Kepler period of $P=21.6^d$ corresponds to a distance of 0.2 AU, which is equal to four magnetospheric radii of RY Tau. In general, if there is more than one planet, wave interference in the accretion disk will lead to a more complex variability pattern.

6. ACKNOWLEDGMENTS

The authors thank S. Yu. Gorda for the spectra obtained at the Kourovka Observatory, A. A. Djupvik for the spectra obtained with the NOT telescope, J. F. Gameiro for the spectra obtained with the CAHA telescope, and D. E. Mkrtchian for the spectra obtained with the TNT telescope.

The authors are grateful for the brightness estimates of RY Tau from the AAVSO international database, provided by observers from around the world and used in this study.

The authors are grateful to M. M. Romanova for discussion of the article and valuable comments.

REFERENCES

- V. Agra-Amboage, C. Dougados, P. J. V. Garcia, and P. Ferruit, *Astron. Astrophys.* **493** (3), 1029 (2009).
- S. H. P. Alencar and G. Basri, *Astron. J.* **119** (4), 1881 (2000).
- S. H. P. Alencar, G. Basri, L. Hartmann, and N. Calvet, *Astron. Astrophys.* **440** (3), 595 (2005).
- S. H. P. Alencar, C. M. Johns-Krull, and G. Basri, *Astron. J.* **122** (6), 3335 (2001).
- N. Arulanantham, M. Gronke, E. Fiorellino, et al., *Astrophys. J.* **944** (2), 185 (2023).
- E. V. Babina, S. A. Artemenko, and P. P. Petrov, *Astron. Lett.* **42** (3), 193 (2016).
- J. Bouvier, *Astron. J.* **99**, 946 (1990).
- J. Bouvier, S. Cabrit, M. Fernandez, and et.al., *Astron. Astrophys.* **272** (1), 176 (1993).
- J. Bouvier, K. N. Grankin, S. H. P. Alencar, et al., *Astron. Astrophys.* **409** (1), 169 (2003).
- J. Bouvier, K. N. Grankin, S. H. P. Alencar, et al., *Protostars and Planets V*, B. Reipurth, D. Jewitt, and K. Keil (eds.), University of Arizona Press, Tucson, 951 (2007).

N. Calvet, J. Muzerolle, C. Briceño, and et.al., *Astron. J.* **128** (3), 1294 (2004).

M. Camenzind, *Reviews in Modern Astronomy* edited by G. Klare **3**, 234 (1990).

M. Cranmer, *Astrophys. J.* **689** (1), 316 (2008).

C. L. Davies, S. Kraus, T. J. Harries, et al., *Astrophys. J.* **897** (1), 31 (2020).

A. V. Dodin and S. A. Lamzin, *Astron. Lett.* **38**, 649 (2012).

W. Fischer, J. Kwan, S. Edwards, and et.al., *Astrophys. J.* **687**, 1117 (2008).

G. F. Gahm, C. Gullbring, K. P. Lindroos, and et.al., *Astrophys. J., Suppl. Ser.* **100**, 371 (1993).

A. Garufi, L. Podio, F. Bacciotti, et al., *Astron. Astrophys.* **628** (2019).

M. S. Giampapa, G. S. Basri, C. M. Johns, and C. Imhoff, *Astrophys. J., Suppl. Ser.* **89**, 321 (1993).

L. Hartmann, G. Herczeg, and N. Calvet, *Annu. Rev. Astron. Astrophys.* **54**, 135 (2016).

L. Hartmann, R. Hewett, and N. Calvet, *Astrophys. J.* **426**, 669 (1994).

W. Herbst, E. J. Grossman, and D. Weinstein, *Astron. J.* **108**, 1906 (1994).

W. Herbst and P. C. Stine, *Astron. J.* **89**, 1716 (1984).

N. Z. Ismailov and A. N. Adygezalzade, *Astron. Rep.* **56**, 131–137 (2012).

N. Z. Ismailov, A. N. Adygezalzade, and G. R. Bahaddinova, *Publications of The Korean Astronomical Society* **30** (2), 229 (2015).

C. M. Johns and G. S. Basri, *Astron. J.* **109**, 2800 (1995).

A. Koenigl, *Astrophys. J., Lett.* **370**, L39 (1991).

R. Kurosawa, M. M. Romanova, and T. J. Harries, *Mon. Not. R. Astron. Soc.* **416**, 2623 (2011).

J. Kwan and W. Fischer, *Mon. Not. R. Astron. Soc.* **411**, 2383 (2011).

A. Lagutin, S. Plachinda, D. Shakhovskoi, and et.al., *Acta Astrophys. Tau.* **1** (1), 33 (2020).

F. Long, G. J. Herczeg, D. Harsono, and P. Pinilla, *The Astrophysical Journal* **882**, 49 (2019).

R. V. E. Lovelace, M. M. Romanova, G. V. Ustyugova, and et.al., *Mon. Not. R. Astron. Soc.* **408**, 2083 (2010).

J. Muzerolle, N. Calvet, L. Hartmann, and et.al., *Astrophys. J.* **550**, 944 (2001).

I. Pascucci, S. Cabrit, S. Edwards, and et.al., *Protostars and Planets VII, ASP Conference Series* **534**, 567 (2023).

K. Perraut, L. Labadie, J. Bouvier, and et.al., *Astron. Astrophys.* **655**, A73 (2021).

P. P. Petrov, *Acta Astrophys. Tau.* **2** (1), 1 (2021).

P. P. Petrov, K. N. Grankin, E. V. Babina, and et.al., *Mon. Not. R. Astron. Soc.* **524** (4), 5944 (2023).

P. P. Petrov, K. N. Grankin, J. F. Gameiro, and et.al., *Mon. Not. Roy. Astron. Soc.* **481**, 132 (2019).

P. P. Petrov, E. Gullbring, I. Ilyin, et al., *Astron. Astrophys.* **341**, 821 (1996).

P. P. Petrov, M. M. Romanova, K. N. Grankin, and et.al., *Mon. Not. R. Astron. Soc.* **504** (1), 871 (2021).

P. P. Petrov, G. V. Zajtseva, Y. S. Efimov, et al., *Astron. Astrophys.* **341**, 553 (1999).

M. M. Romanova and S. P. Owocki, *Space Sci. Rev.* **191**, 339 (2015).

M. M. Romanova, G. V. Ustyugova, A. V. Koldoba, and et.al., *Mon. Not. R. Astron. Soc.* **399**, 1802 (2009).

F. Shu, J. Najita, E. Ostriker, and et.al., *Astrophys. J.* **429**, 781 (1994).

S. L. Skinner, M. Audard, and M. Güdel, *Astrophys. J.* **826**, 15 (2016).

S. L. Skinner, P. C. Schneider, M. Audard, and et.al., *Astrophys. J.* **855**, 143 (2018).

G. St-Onge and P. Bastien, *Astrophys. J.* **674**, 1032 (2008).

M. Takami, H. M. Gunther, P. C. Schneider, and et.al., *ApJ SS* **264**, 1 (2023).

M. Takami, Y. J. Wei, M. Y. Chou, and et.al., *Astrophys. J.* **820** (2), 139 (2016).

S. Takasao, K. Tomida, K. Iwasaki, and et.al., *Astrophys. J.* **941** (1), 29 (2022).

G. V. Ustyugova, A. V. Koldoba, M. M. Romanova, and et.al., *Astrophys. J.* **646**, 304 (2006).

S. D. Vedula and C. Johns-Krull, *Bulletin of the American Astronomical Society* **56** (2) (2024).

G. V. Zajtseva, *Astrophysics* **53**, 212 (2010).

G. V. Zajtseva, Y. Efimov, P. Petrov, and et.al., *ASP Conf. Ser.* 154, *The Tenth Cambridge Workshop on Cool Stars, Stellar Systems and the Sun*, Edited by R. A. Donahue and J. A. Bookbinder p. 1808 (1996).

Time lag between accretion and wind events in the T Tauri star RY Tau

E. V. Babina¹, P. P. Petrov¹, K. N. Grankin¹, S. A. Artemenko¹

¹Crimean Astrophysical Observatory, RAS, Republic of Crimea, 298409 Russia

Results of spectroscopic and photometric monitoring of the Classical T Tauri type star RY Tau are presented. The observations cover a time interval since 2013 to 2024, a total of 220 nights. During the observations, the brightness of the star varied within the range of $V=9-11^m$. The rotation axis of the "star + accretion disk" system is inclined at a large angle, so that the line of sight intersects both the region of the wind and the accreting flows in the magnetosphere of the star. Variability of the flux in the shortwave wing of the $H\alpha$ emission line and variability of the D NaI resonance doublet profile are analyzed. It is shown that the wind and accretion fluxes vary on a time scale of about 20-24 days. When the flow direction changes, a time lag is observed: first, accretion increases, and after two days, absorption in the wind along the line of sight decreases. It is concluded that the spectral line profiles are formed in magnetospheric accretion flows and in the conical wind starting from the magnetosphere boundary. The time lag is determined by the tilt of the magnetic dipole and the opening angle of the conical wind. It is suggested that RY Tau is in an unstable propeller mode, with fluctuations in the accretion and wind flows caused by density waves in the accretion disk.

Keywords: *Stars: variables: T Tauri, Herbig Ae/Be – Stars: winds, outflows – Line: profiles – Stars: individuals: RY Tau*